

# Friction on incommensurate substrates: Role of anharmonicity and defects

S. Amiri, C.A. Volkert, and R.L.C. Vink

*Institute of Materials Physics, Georg-August-Universität Göttingen, 37073 Göttingen, Germany*

(Dated: May 25, 2022)

We present Molecular Dynamics simulations of one- and two-dimensional bead-spring models sliding on incommensurate substrates. We investigate how sliding friction is affected by interaction anharmonicity and structural defects. In their absence, we confirm earlier findings, namely, that at special resonance sliding velocities, friction is maximal. When sliding *off-resonance*, partially thermalized states are possible, whereby only a small number of vibrational modes becomes excited, but whose kinetic energies are already Maxwell-Boltzmann distributed. Anharmonicity and defects typically destroy partial thermalization, and instead lead to full thermalization, implying much higher friction. For sliders with periodic boundaries, thermalization begins with vibrational modes whose spatial modulation is compatible with the incommensurate lattice. For a disc-shaped slider, modes corresponding to modulations compatible with the slider radius are initially the most dominant. By tuning the mechanical properties of the slider's edge, this effect can be controlled, resulting in significant changes in the sliding distance covered.

## I. INTRODUCTION

A sliding object generally loses its kinetic energy of forward motion and slows down due to friction. Understanding friction is still elusive in the majority of applications, for, if friction were understood, we would likely not be spending 20% of our energy consumption at trying to overcome it [1]. The loss of energy due to friction, by which one really means the conversion of useful energy (e.g. forward kinetic motion) into less useful forms (e.g. heat), can occur via many channels (phononic, electronic, magnetic, electrochemical, to name but a few [2–6]). One of these channels, the one we focus on in this paper using molecular dynamics simulations, is the phononic channel, i.e. the loss of useful energy via the generation of internal lattice vibrations. The origins of phononic friction have been, and still are, actively discussed [3, 7–11]. One view is that phonon scattering processes play a crucial role. Hence, materials with large anharmonicities in their interactions, or containing scattering centers such as structural defects, are likely to be more dissipative than materials without these properties [7].

Indeed, Molecular Dynamics (MD) simulations confirm that phonon scattering processes can be a major cause of energy dissipation under sliding, and the dissipation rate can be quantitatively related to phonon lifetimes [12]. The results of Ref. [12] were obtained using a 3D setup, consisting of an FCC copper substrate coated with a single layer of graphene, with a second graphene layer being dragged across the coated layer. The frictional properties could then be related to the lifetimes of phonons generated in the dragged graphene layer.

The setup of Ref. [12] resembles a 2D Frenkel-Kontorova (FK) model [13], such as studied in Ref. [14]. The essential difference is that, in the FK model, only in-plane particle motion of the sliding layer is retained, i.e. the dynamics is strictly 2D. Nevertheless, even with this simplification, friction is higher when the particle interactions include some degree of anharmonicity, im-

plying shorter phonon lifetimes [15]. In another simulation study carried out by one of us [16], friction depended quite strongly on whether the substrate interactions were harmonic or not, being clearly correlated with the phonon lifetime (here: of phonons in the substrate, not in the slider, which in Ref. [16] was a point particle). Further recent experimental studies also identify the phonon lifetime as key factor determining friction [17, 18].

The aim of this study is to further focus on the role of phonon scattering on sliding friction, considering interaction anharmonicity and structural defects. We will do so using the FK model, for which a large body of results is already available [14, 19, 20]. We bring the system into an initial sliding state, then monitor how the kinetic energy of forward motion is converted into internal lattice vibrations, i.e. heat. Our results apply to the FK model in its “floating” state, i.e. in the absence of static friction. Such states can be realized using systems sliding on incommensurate substrates, and where the coupling to the substrate is weak (i.e. below the Aubry transition [21–23]). The accepted view is that such systems, provided they are large enough, once brought into a sliding state, eventually thermalize, i.e. with the initial kinetic energy of forward motion having been converted entirely into heat [14, 19, 20, 24]. However, depending on the precise system parameters (in particular, the initial sliding velocity [19]), thermalization can be very slow. Possible experimental realizations could be small crystalline clusters (graphene flakes) sliding on incommensurate crystalline surfaces [25, 26], clusters of Xe atoms sliding on Ag(111) substrates [24, 27], or trapped ions in optical lattices [23].

## II. MODEL AND METHODS

We consider FK models in  $d = 1$  (1D) and  $d = 2$  (2D) dimensions. For the 1D case, a large body of theoretical results is available (in particular Ref. [19]) which help to guide the simulations, also in 2D. As stated previously, the extension of this work is to include additional phonon

scattering processes, by means of anharmonicity and defects.

### A. 1D FK model

The 1D model considers a chain of  $i = 1, \dots, N$  atoms, confined to move along a line, where periodic boundary conditions are applied. Each atom (uniform single atom mass  $m$ ) in the chain is connected by springs to its two nearest neighbors. The energy of a single spring is given by

$$u_{\text{spr}}(r) = \sum_{n=2}^4 \epsilon \alpha_n (r/a - 1)^n, \quad (1)$$

where  $r$  denotes the distance between the two atoms participating in the bond,  $a$  the equilibrium bond length, and where  $\epsilon$  sets the energy scale. We will, in what follows, speak of harmonic and anharmonic systems. For the harmonic system, we use  $\alpha_2 = 36, \alpha_3 = \alpha_4 = 0$ ; for the anharmonic system  $\alpha_2 = 36, \alpha_3 = -252, \alpha_4 = 1113$ . These parameters stem from a Taylor expansion of a (12, 6) Lennard-Jones potential around its minimum, with the minimum located at  $r = a$ , and well-depth  $\epsilon$ .

The total length of the system  $L = aN$  such that, in the absence of any external fields, the chain ground-state energy equals zero. In addition to the mobile chain, an array of  $M = \text{int}(gN)$  evenly-spaced static particles is distributed along the line, with  $g = (1 + \sqrt{5})/2$  the golden ratio, and where “int” means rounding down to the nearest integer. This choice ensures maximum incommensurability between the mobile chain and the static obstacles [14], while remaining compatible with the periodic boundaries. The static obstacles interact with the mobile chain atoms via a soft pair potential of the form:

$$u_{\text{soft}}(r) = \begin{cases} \alpha \epsilon \left[ 1 + \cos\left(\frac{\pi r}{r_c}\right) \right] & r < r_c \\ 0 & \text{otherwise,} \end{cases} \quad (2)$$

with  $\alpha = 0.3$  and  $r_c = L/(2M)$ . The use of an incommensurate static potential, and the relatively weak coupling between static layer and chain, ensures a “floating” state, whose friction is expected to be minimal (that is, we always stay below the Aubry transition [21–23], i.e. there is no static friction).

The undeformed chain (i.e. with all the springs at their equilibrium length  $a$ ) is placed on the line containing the obstacles (a random uniform displacement is applied to all chain atoms, in order to sample different initial starting positions). At time  $t = 0$ , the chain is “kicked” by assigning each chain atom the same velocity  $v_K$  along the chain direction; the subsequent chain dynamics is then obtained by time-integrating the equations of motion in the micro-canonical ( $NVE$ ) ensemble. Directly after kicking, the velocity of the chain center of mass equals  $v_K$ . However, due to the generation of vibrations in the chain (caused by collisions with the static

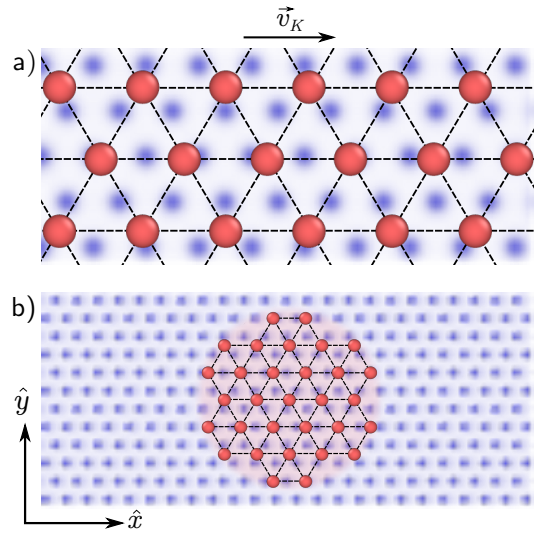


FIG. 1. Schematics of the 2D FK model. Red circles represent the mobile atoms, which form a hexagonal lattice, whereby each atom is connected to its nearest neighbors by springs (dashed lines). The blue circles (blurred) represent the static obstacles which generate the potential energy landscape through which the mobile layer slides. The layer of mobile atoms is kicked with velocity  $v_K$  along the  $x$ -axis, as indicated. We consider two geometries: a) sliding layer which is fully periodic in both dimensions, and b) a finite patch of sliding atoms (flake), approximately disc shaped.

obstacles, as well as, for the anharmonic chain, via internal phonon scattering) the velocity of the chain center of mass will typically decrease with time, i.e. there is friction. We emphasize that no thermostat is applied in these simulations. Hence, results are completely free from thermostat-induced artifacts, which in friction simulations can be quite strong [16, 28, 29]. The present approach thus facilitates an unbiased view into the origins of sliding friction, using what is arguably the optimally simplified “minimal” model.

### B. 2D FK model

The 2D model uses hexagonal lattices for both the mobile atoms and the static obstacles, with periodic boundaries applied in both directions. We consider two geometries, namely a fully periodic slider, and a finite patch (flake) of sliding atoms [Fig. 1]. For the fully periodic system, the mobile lattice contains  $i = 1, \dots, N$  atoms, single atom mass  $m$ , each atom connected to its six nearest neighbors by springs. The aspect ratio of the lattice  $L_y/L_x = \sqrt{3}/2$ , with  $L_i$  the length of the system in the direction  $i \in x, y$ . The single spring energy is given by Eq. (1), the spring rest length equals the lattice constant  $a$ . The same definitions of harmonic and anharmonic bonds as used for the 1D chain are applied here as well. For the static incommensurate potential energy landscape,  $M = \text{int}(g^2N)$  static particles are arranged

on a second hexagonal lattice, using the same aspect ratio  $L_y/L_x$  as the mobile lattice, where  $g$  is the golden ratio. In this way, the ratio of lattice constants  $a/a_c$  is as close as possible to  $g$ , where  $a_c$  is the lattice constant of the static layer, ensuring maximum incommensurability. The interaction between the static obstacles and the mobile atoms is again of the form of Eq. (2), with  $\alpha = 0.3$  and  $r_c = a_c/2$ . The 2D hexagonal layer of mobile atoms is placed inside the static potential energy landscape generated by the obstacles, oriented as shown in Fig. 1(a). At time  $t = 0$ , all the atoms in the mobile layer are “kicked”, by assigning them the velocity  $v_K$  in the  $\hat{x}$  direction (prior to kicking, the mobile lattice is given a random uniform 2D displacement, in order to sample different starting positions). We emphasize that the model is purely 2D, i.e. the mobile atoms can move in the  $\hat{x}$  and  $\hat{y}$  directions only. Immediately after kicking, the motion is entirely in the  $\hat{x}$  direction, but soon thereafter, due to collisions with the static obstacles, also motion in the  $\hat{y}$  direction develops. For the flake, a finite portion of the hexagonal lattice is retained, keeping only those atoms inside a specified radius of some central reference atom [Fig. 1(b)]. Most of the flake atoms will be six-fold coordinated, except for those on the edge, which have missing bonds. The flake is oriented with respect to the static lattice in the same way as the fully periodic slider. The static lattice is chosen large enough to fully encompass the flake, such that periodic boundary conditions may safely be applied.

### C. Units

For both the 1D and 2D model, length is expressed in units of the equilibrium lattice constant  $a$ , energy in units of  $\epsilon$ , particle mass in units of some reference mass  $m^*$ , and temperature in units of  $\epsilon/k_B$ , with  $k_B$  the Boltzmann constant. This implies time unit  $[t] = \sqrt{m^*a^2/\epsilon} \sim 2.6$  ps assuming a sliding layer consisting of C-atoms ( $a \approx 3.8$  Å,  $m^* \approx 12$  u,  $\epsilon \approx 2.76$  meV/atom [30]).

### D. Eigenmodes

To analyse the vibrational excitations in the mobile lattice induced during sliding, we use the language of eigenmodes, which has proven to be useful in other studies also [31]. For a system of  $i = 1, \dots, N$  particles, there are  $k = 1, \dots, dN$  eigenmodes, with  $d = 1, 2$  the spatial dimension of the problem at hand. The eigenmodes follow in the usual way from the (mass-weighted) hessian,  $H_{\mu\nu} = \frac{1}{\sqrt{m_\mu m_\nu}} \frac{\partial^2 E}{\partial \mu \partial \nu}$ , with  $E$  the total spring energy of the system given by Eq. (1), and with the derivatives evaluated with the sliding atoms in their perfect equilibrium lattice positions (of course, when computing the hessian, the interaction with the static particles is excluded). The labels  $\mu, \nu$  refer to the set of all Cartesian coordinates of

the particles,  $m_{\mu,\nu}$  being the associated particle mass. The hessian is a  $dN \times dN$  matrix, but most elements are zero, since the particles interact only with nearest neighbors. Upon diagonalization of the hessian, a set of eigenvectors  $\vec{\xi}_k$  is obtained, each one with an associated eigenfrequency  $\omega_k^2$ . For the 1D chain, there is exactly one mode with zero eigenfrequency, corresponding to a global translation of the chain along the  $x$ -axis. For the 2D sliding layer, there will always be at least two zero frequency modes, corresponding to global translations in the two lateral directions. In addition, if the 2D layer is a finite patch, there will also be a third zero frequency mode, corresponding to a global rotation. For lattices with perfect translational symmetry (i.e. fully periodic, defect-free crystals), one can assign a wavevector to each eigenmode, then corresponding to a true phonon.

During the sliding simulations, we record, for each particle, the displacement  $\vec{u}_i(t)$  from the initial (perfect lattice) position, and velocity  $\vec{v}_i(t)$ , both as functions of time  $t$  (for the 1D chain, these quantities are scalars; for the 2D sliding layer, they are 2D vectors). From these, we define the kinetic energy of the  $k$ -th eigenmode as:

$$K_k(t) = \frac{1}{2} \left( \sum_{i=1}^N \sqrt{m_i} \vec{v}_i(t) \cdot \vec{\xi}_{k,i} \right)^2, \quad (3)$$

with the sum over all particles,  $m_i$  the mass of particle  $i$ , and  $\vec{\xi}_{k,i}$  the sub-vector of the full eigenvector  $\vec{\xi}_k$ , containing only the components of particle  $i$ . Defined in this way, one consistently has

$$E_{\text{kin}} = \sum_{i=1}^N \frac{m_i \vec{v}_i^2}{2} = \sum_{k=1}^{dN} K_k, \quad (4)$$

which holds exactly (for both harmonic and anharmonic systems).

## III. RESULTS

All our MD results were obtained with LAMMPS [32]; implementation details are provided in the Appendix.

### A. 1D chain

We consider a chain with  $N = 100$  particles, periodic boundaries, unit particle mass  $m = 1$ . Unless stated otherwise, the bond interaction of Eq. (1) is harmonic. For these parameters, the frictional behavior is well understood [19]. The static obstacles induce a spatial modulation of wavenumber  $k^* = 2\pi/a_c$  in the chain [33], with  $a_c$  the lattice spacing of the static obstacles. The chain center of mass motion thus couples to the chain internal vibrations via the mode  $k^*$ ; the associated vibrational frequency follows from the dispersion relation  $\omega^* = 2\sqrt{2\alpha_2\epsilon/m} |\sin(ak^*/2)|$ . When kicked with velocity

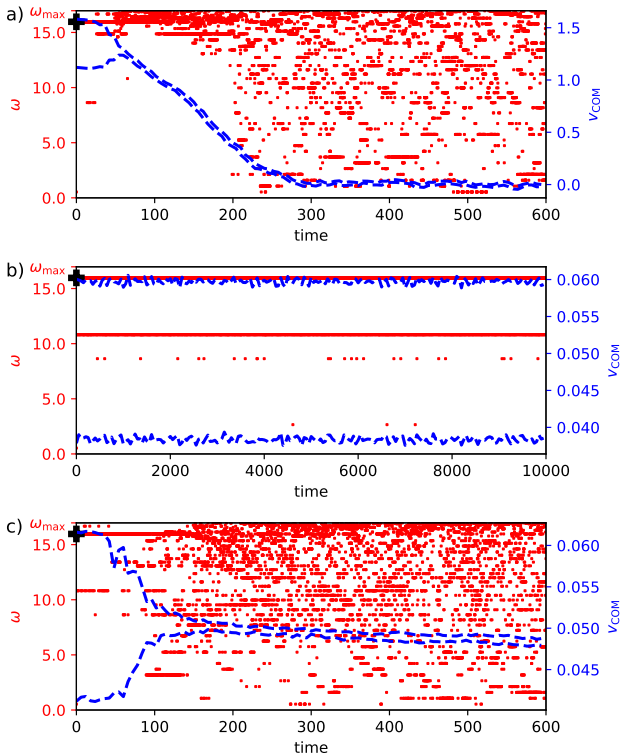


FIG. 2. 1D sliding chain results, showing time evolution directly after kicking with velocity  $v_K$  (results averaged over 20 trajectories, each with different initial position of the slider). The dashed blue curves show the lower and upper envelope of the chain center of mass velocity  $v_{\text{COM}}$ . The red dots indicate, for each time step, the frequency of the kinetically most active mode. Symbol + on the vertical axes indicates  $\omega^*$ ; the maximum mode frequency  $\omega_{\text{max}} \approx 16.97$ . (a) Harmonic chain kicked with the resonance velocity  $v_K^*$ . The decay of  $v_{\text{COM}}$  sets in rapidly after kicking. (b) Harmonic chain kicked with  $v_K = 0.05 \ll v_K^*$ . In this case,  $v_{\text{COM}}$  oscillates between a low and high value, but there is no decay. Only a small subset of available modes reveals noticeable activity. (c) Same as b), but using *anharmonic* interactions. The decay of  $v_{\text{COM}}$ , and subsequent thermalization, commence rapidly after kicking.

$v_K$ , chain atoms “hit” the obstacles with the washboard frequency  $\Omega = v_K/a_c$ . Friction arises when a resonance is created,  $2\pi\Omega \sim \omega^*$ . Via a cascade of couplings between  $k^*$  and the other vibrational modes in the chain, the kinetic energy of the center of mass forward motion is transferred, via  $k^*$ , to the entire population of chain vibrational modes, thereby converted into heat.

For our model parameters  $\omega^* \approx 15.97$ , the corresponding resonance kick velocity  $v_K^* \approx 1.58$ . When the chain is kicked with  $v_K^*$ , the chain center of mass velocity decays rapidly with time, i.e. friction is high [Fig. 2(a)]. In contrast, using  $v_K = 0.05$ , which is far below resonance,  $v_{\text{COM}}$  oscillates between a low and high value, but there is no sign of any decay, i.e. friction is low [Fig. 2(b)]. Also indicated in Fig. 2 is the frequency of the kinetically most

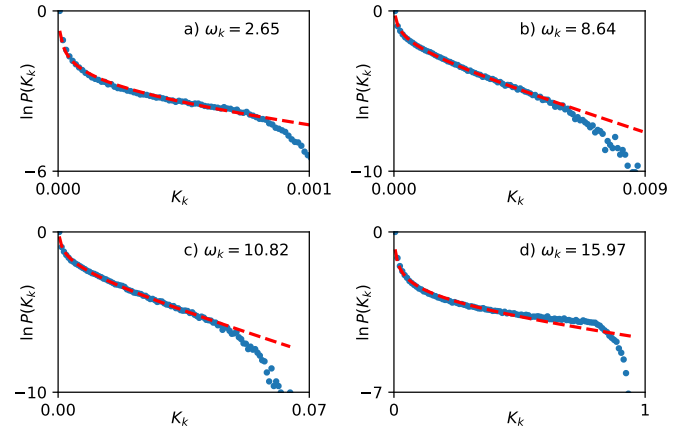


FIG. 3. 1D *harmonic* chain results, showing the logarithm of the distribution of mode kinetic energies, obtained during sliding in the low-friction state of Fig. 2(b). Results are shown for the four most active modes, with frequencies  $\omega_k$  as indicated. The dashed lines show fits to Eq. (5), which are two-parameter fits, one of them being the mode temperature  $T_k$ .

active mode as a function of time, defined as the mode having the highest value of  $K_k$ , as given by Eq. (3). In the low-friction state, Fig. 2(b), only a few modes are active. These are the modes  $k^*$ , as well as some of the *higher harmonics*, corresponding to wavenumber  $nk^*$ , with  $n$  a positive integer. In the high-friction state, Fig. 2(a), at very early times, we also observe that activity is concentrated around  $k^*$ , but soon spreads to all modes, reminiscent of a system in thermal equilibrium (the signal  $K_k$  then essentially being a random variable).

The low-friction state of Fig. 2(b) can persist because, being *off-resonance*, the coupling of  $k^*$  to other vibrational modes is weak, *and* because the chain interaction is harmonic (i.e. no scattering between modes). In such a highly de-coupled system, the transfer of energy between modes is severely hampered, meaning that thermalization (i.e. generation of heat) cannot occur, which explains why friction is low. Indeed, by using *anharmonic* bonds, which enable mode scattering thereby assisting thermalization, the second condition no longer holds, and the low-friction state is no longer observed [Fig. 2(c)].

Next, we address thermalization. The low-friction state of Fig. 2(b) is not thermalized, since only a small subset of modes is active. Nevertheless, precursors to thermalization are already present. To see this, we consider the four most active modes of Fig. 2(b), whose wavenumbers are  $k = nk^*$ , with  $n = 1, 2, 3, 5$  (i.e. the fundamental mode, and some of the leading higher harmonics, excluding  $n = 4$ , which showed very little activity). The respective vibrational frequencies are  $\omega_k = 15.97; 10.82; 8.64; 2.65$ . For these modes, while sliding in the low-friction state, the distribution (histogram) of observed kinetic energy values  $K_k$  is recorded. In a perfectly thermalized system, these values are Maxwell-Boltzmann

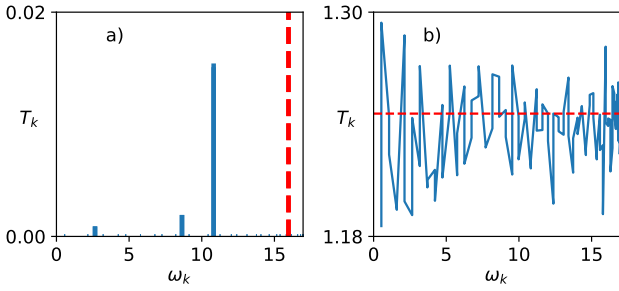


FIG. 4. 1D *harmonic* chain results, showing mode temperatures  $T_k$  obtained by fitting to Eq. (5), as function of the mode frequency  $\omega_k$ . a) As obtained in the low-friction state of Fig. 2(b). Note:  $T_k$  for the principal mode  $k^*$  (dashed line) far exceeds the vertical range of the graph. b) As obtained in the long-time limit after kicking with the resonance velocity  $v_K^*$ ; dashed line marks the equipartition temperature.

distributed,  $P_{\text{th}} \propto e^{-K_k/k_B T_k}$ , with  $T_k$  the mode temperature, and  $k_B$  the Boltzmann constant. In a perfectly coherent state,  $K_k$  as function of time is strictly harmonic, at *twice* the mode frequency, in which case the distribution takes the form  $P_{\text{coh}} \propto K_k^{-1/2}$ , valid in the limit of small  $K_k$  (Appendix). However, the low-friction state considered here is neither fully thermalized nor coherent, and so we expect a *hybrid* form:

$$P(K_k) = P_{\text{th}} \cdot P_{\text{coh}} \propto e^{-K_k/k_B T_k} / \sqrt{K_k} \quad (5)$$

We test the validity of Eq. (5) in Fig. 3, for each of the four most active modes. The dashed curves are fits using Eq. (5). Overall, the fits capture the data well. In all cases, agreement breaks down at large values of  $K_k$ , since, on the one hand, Eq. (5) is a small  $K_k$  approximation, but, more importantly, due to bad statistics (large values of  $K_k$  are exponentially suppressed by the Maxwell-Boltzmann factor, so these values do not appear very often in the simulation time series).

We repeat the analysis of Fig. 3 for all modes  $k$  in the chain, to obtain the mode temperatures  $T_k$ . In the low-friction state, there are just a few active modes with finite temperature, inside a background of frozen modes [Fig. 4(a)]. The partial thermalized character of the low-friction state is clearly visible: While individual modes already have energy distributions conforming to Maxwell-Boltzmann, the corresponding temperatures between modes are very different. Fig. 4(b) shows the mode temperatures  $T_k$  obtained after kicking with the resonance velocity  $v_K^*$ , in the long-time limit where  $v_{\text{COM}} \sim 0$ . We now observe a much more homogeneous temperature distribution, all modes having essentially the same temperature, showing that the chain has fully thermalized. For the *harmonic* chain in thermal equilibrium, equipartition should hold, i.e. the initial kinetic energy of the kick ( $K_{\text{in}} = mNv_K^2/2$ ) should be equally divided over all system degrees of freedom ( $\text{ndof} = 2dN$ ,

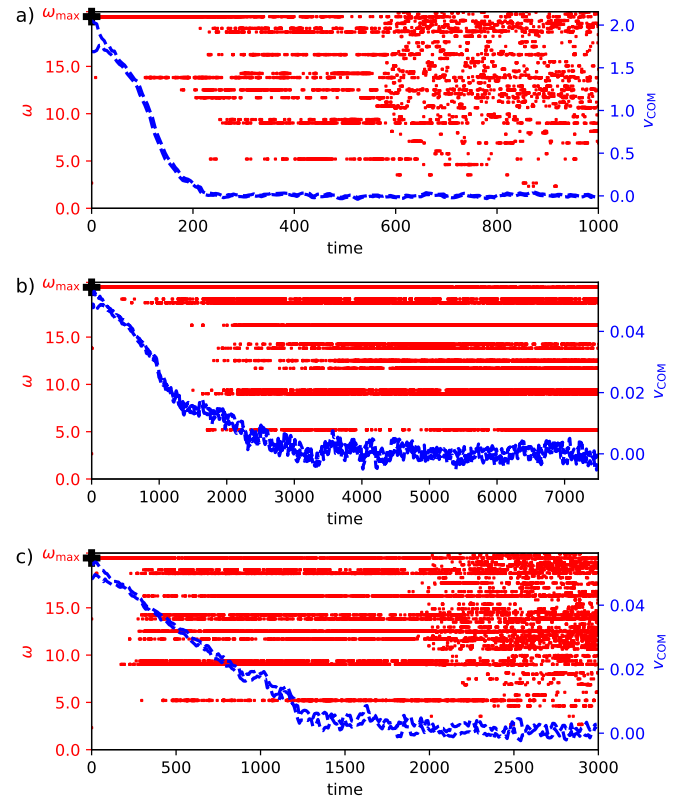


FIG. 5. Sliding behavior of the 2D fully periodic slider (results are averaged over 20 different initial positions of the slider). The representation of the data is the same as in Fig. 2. Symbol + indicates the frequency  $\omega^*$  of the dominant mode  $k^*$ , the maximum possible mode frequency  $\omega_{\text{max}} \approx 20.78$ . Results are shown for a) harmonic interactions at the resonance kick velocity  $v_K^*$ , b) harmonic interactions at  $v_K = 0.05$ , and c) *anharmonic* interactions at  $v_K = 0.05$ .

with  $d = 1$  the spatial dimension; factor two counts position and momentum degrees of freedom). For the harmonic chain in equilibrium,  $k_B T/2 = K_{\text{in}}/\text{ndof}$ , implying  $T \approx 1.246$  in our units, which Fig. 4(b) confirms.

## B. 2D hexagonal layer

### 1. 2D fully periodic slider without defects

We first consider a 2D sliding layer with full periodic boundary conditions, i.e. in the absence of any free edges or other defects [Fig. 1(a)]. A layer of  $N = 196$  mobile atoms, unit particle mass  $m = 1$ , is “kicked” at time  $t = 0$  with velocity  $v_K$  in the  $\hat{x}$ -direction. For this value of  $N$ , the lattice constant of the static obstacles  $a_c = 7a/11$ . In analogy with the 1D chain, we assume that the static obstacles induce a spatial modulation of wavevector *magnitude*  $k^* = 2\pi/s$ , with  $s = a_c \sin 60^\circ$  the spacing between closed-packed rows of obstacles, see Fig. 1(a). As for the *direction* and *polarization*, we assume that longitu-

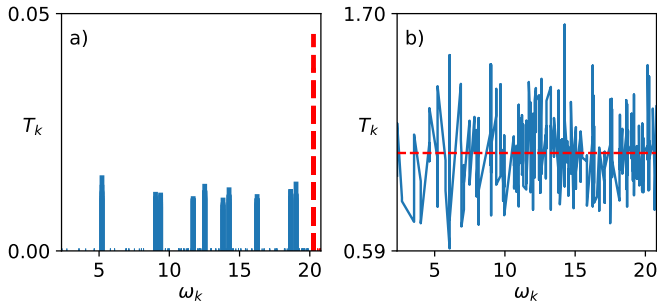


FIG. 6. The analogue of Fig. 4, but for the 2D periodic slider with harmonic bonds. a) As obtained in the partially thermalized state of Fig. 5(b), where the slider was kicked with an *off-resonance* velocity  $v_K = 0.05$ . b) As obtained in the long-time limit of Fig. 5(a), where the slider was kicked with the resonance velocity  $v_K^*$ . In this case, there is full thermalization.

dinal modes propagating at  $\pm 30^\circ$  relative to  $\hat{x}$  will be the dominant excitation. The corresponding vibrational frequency  $\omega^* \approx 20.26$ , which follows from the dispersion relation (Appendix). For sliding in the  $\hat{x}$ -direction, the washboard frequency  $\Omega = v_K/a_c$ , implying resonance kick velocity  $v_K^* \approx 2.05$ .

For the slider with harmonic bonds, the decay of  $v_{\text{COM}}$  with time at the resonance kick velocity  $v_K^*$  is shown in Fig. 5(a), while Fig. 5(b) shows the result for  $v_K = 0.05$ , i.e. far below resonance. In agreement with the 1D chain, the decay is most rapid at resonance, i.e. friction is highest there. In addition, strong initial activity of the mode  $k^*$  is observed, confirming the above assumption that longitudinal modes propagating at  $\pm 30^\circ$  couple most strongly to the center of mass motion (the other plateaus visible in Fig. 5 correspond to higher harmonics  $nk^*$ ). Regarding as to how the energy gets distributed over the vibrational modes, there is an important qualitative difference with the 1D chain. In 2D, see Fig. 5(b), a state is observed where  $v_{\text{COM}} \sim 0$ , while the vibrational modes are still far from thermal equilibrium. This state is analogous to the low-friction state of Fig. 2(b), the crucial difference being that, in 2D,  $v_{\text{COM}} \sim 0$ , i.e. the system is no longer sliding. Repeating the simulation using  $v_K = 0.05$  and *anharmonic* bonds, Fig. 2(c), we observe a slightly more rapid decay of  $v_{\text{COM}}$  compared to the harmonic case at the same kick velocity, but this time the system fully thermalizes, i.e. all modes become active.

For the harmonic sliders, we still verify the degree of thermalization. For the slider in the partially thermalized state, Fig. 5(b), mode activity is mainly restricted to  $k^*$  and the higher harmonics. As in the 1D case, the kinetic energy distributions of these modes already appear thermalized, i.e. well described by Eq. (5). In Fig. 6(a), we plot the corresponding mode temperatures, which reveals many frozen modes ( $T_k \sim 0$ ), and a number of active modes ( $T_k > 0$ ), confirming that the state is indeed partially thermalized (for a fully thermalized state,

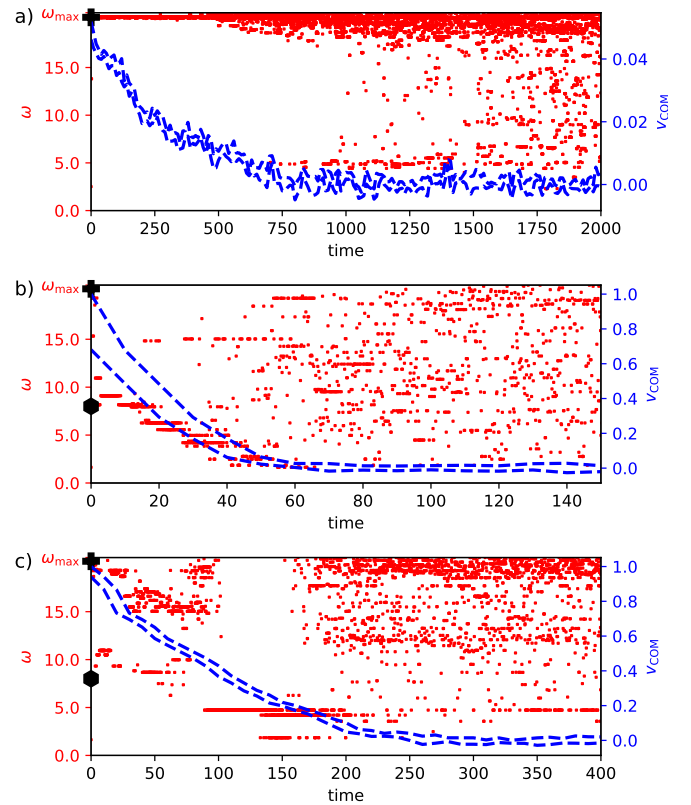


FIG. 7. 2D *harmonic* sliders containing defects (results are averaged over 20 different initial positions of the slider). The representation of the data is the same as in Fig. 2. Symbol + indicates  $\omega^*$  of the modulation  $k^*$  induced by the static obstacles; symbol  $\circ$  indicates  $\omega_R$  induced by the slider radius. a) Fully periodic slider with a fraction 2% of randomly selected missing bonds, at kick velocity  $v_K = 0.05$ . b) Sliding patch (flake) kicked with velocity  $v_K = 1$ . c) Same as b), but for a slider with rigid edge.

$T_k$  should be the same for all modes). Compared to the analogous 1D case, Fig. 4(a), we find that in 2D the mode temperature is more homogeneous (with the exception of  $\omega^*$ , the active modes have similar temperatures). In Fig. 6(b), we show the mode temperatures for the slider kicked with the resonance velocity  $v_K^*$ , i.e. corresponding to Fig. 5(a), in the long-time limit. In this case, the system fully thermalizes, all mode temperatures being the same. Note that equipartition is obeyed quite well,  $k_B T_{\text{eq}} = m(v_K^*)^2/4 \approx 1.05$ , as indicated by the dashed horizontal line. For the anharmonic slider, Fig. 5(c), the system also fully thermalizes, but this comes as no surprise, due to the enhanced phonon scattering induced by anharmonicity (result therefore not shown).

## 2. 2D slider with defects

We now investigate the role of lattice defects on the sliding behavior, considering bond and edge defects. For

the bond defects, we remain with the fully periodic slider considered previously (same number of particles  $N = 196$ ; unit particle mass  $m = 1$ ) but with a fraction 2% of randomly selected bonds removed from the lattice (we checked that, for this low fraction, the lattice remains a single connected entity, i.e. there are no isolated atoms without any bonds). Fig. 7(a) shows the corresponding sliding behavior, using harmonic interactions and kick velocity  $v_K = 0.05$ , to be compared to the corresponding defect-free case of Fig. 5(b). The difference is striking: Whereas the defect-free slider did not thermalize, the presence of just a small number of defects strongly promotes thermalization, implying a much higher friction. Mode activity at short times is still concentrated around the dominant mode  $k^*$ , but enhanced activity of the higher harmonics is no longer observed. Apparently, the presence of just a small number of defects is sufficient to destroy the coupling between  $k^*$  and its higher harmonics.

To study the influence of edge defects, we consider a disc-shaped slider (flake), see Fig. 1(b). The flake contains  $N = 199$  particles, i.e. comparable to the fully periodic system; unit particle mass  $m = 1$ . The edge of the slider provides an additional source of phonon scattering, which dramatically reduces sliding. In fact, at low kick velocity,  $v_K = 0.05$ , the flake refuses to slide at all, merely a damped rocking motion of the center of mass is observed, irrespective of whether harmonic or anharmonic bonds are used. The damping is very strong, and the system thermalizes rapidly (results not shown). To observe any sliding at all, higher kick velocities are required. In Fig. 7(b), we show results for  $v_K = 1$ , using harmonic interactions. We find that the system thermalizes extremely rapidly, even faster than the fully periodic slider at the resonance velocity  $v_K^*$  [cf. Fig. 5(a)]. Note also that initial mode activity is no longer concentrated at  $\omega^* \approx 20.26$  induced by the static obstacles, but instead at a much lower frequency. For the flake, the dominant spatial modulation is set by the flake radius,  $k_R \sim 2\pi/R$ , where  $R \sim 6.9a$  presently. From the dispersion relation, and assuming longitudinal modes at  $\pm 30^\circ$  still dominate, this leads to a vibrational frequency  $\omega_R \sim 8$ , which is indeed rather close to the frequency where initially much activity is observed, see Fig. 7(b). By making the edge of the slider infinitely stiff (i.e. treat the edge as a rigid object, while time-integrating the internal particles as before, some of which with bonds to the, now rigid, edge) one can reduce the spatial modulation  $k_R$ . In this case, still kicking with velocity  $v_K = 1$ , the decay of  $v_{\text{COM}}$  can be postponed, see Fig. 7(c). Note that, by reducing the modulation  $k_R$ , the modulation  $k^*$  becomes visible again, leading to initial mode activity at both frequencies,  $\omega_R$  and  $\omega^*$ , simultaneously.

As possible control tactic to reduce friction, the results of the sliding flake suggest optimizing the mechanical properties of the slider, in order to reduce the spatial modulation  $k_R$  induced by the finite system size. As shown above, one way this may be achieved is to make

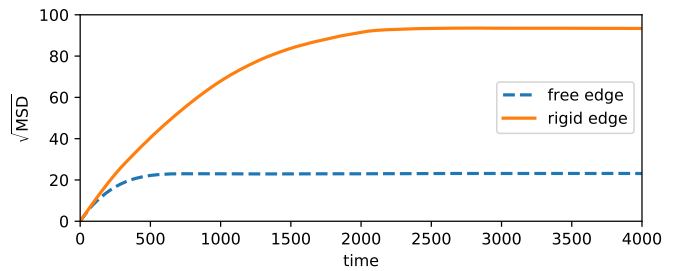


FIG. 8. Total sliding distance versus time, as expressed via the mean-squared-displacement, for the flake with free and rigid edge. All interactions are harmonic, the kick velocity  $v_K = 1$ .

the edge of the slider as stiff as possible (rigid). This results in a significant increase of the covered sliding distance,  $s = \sqrt{\text{MSD}}$ , where MSD is the mean-squared-displacement of the slider atoms, as measured from the time of the kick [Fig. 8]. As the figure shows, the slider with the rigid edge slides roughly five times further.

#### IV. CONCLUSIONS

We have investigated the sliding behavior of 1D and 2D bead-spring models on incommensurate substrates, in the “floating” state, i.e. below the Aubry transition. For the 1D system, our results are fully consistent with the theoretical predictions of Ref. [19]. For harmonic chain interactions, friction is highest when the washboard frequency corresponding to the kick velocity  $v_K$  resonates with the dominant vibrational mode induced by the incommensurate substrate. For  $v_K$  chosen *off-resonance*, a low-friction state is possible, where the system slides seemingly indefinitely, with only a small subset of the system vibrational modes showing any activity. As was already known [19], the low-friction state can only survive in sufficiently small systems, such that the vibrational spectrum remains discrete. One insight of this work is that, in addition, the interactions must be sufficiently harmonic, since anharmonicity will also destroy the low-friction state. A further insight is that the low-friction state is already partially thermalized, the kinetic energies of the active vibrational modes being well described by a modified Maxwell-Boltzmann factor. Thermal fluctuations (i.e. randomness) are thus already present, which could imply that the low-friction state unavoidably has a finite lifetime.

In 2D, for the system size considered here, a low-friction state where the system slides indefinitely, was not observed. This is consistent with Ref. [14], where it was also found that true 2D models typically equilibrate, rather than slide, even when the system size is small. Instead, we find that partially thermalized states are possible, with only a few active vibrational modes, but where the center of mass velocity has already de-

cayed to zero. These partially thermalized states can occur when the system is kicked with an *off-resonance* velocity, and for harmonic interactions. In line with the 1D system, the kinetic energies of the active modes are Maxwell-Boltzmann distributed, so thermal fluctuations already manifest themselves. For anharmonic interactions, the partially thermalized state is also observed, but here its duration is very brief, full thermalization setting in quickly.

For both the 1D and 2D periodic sliders, but without defects, the vibrational modes that initially get excited correspond to the dominant spatial modulation induced by the incommensurate substrate and higher harmonics. In the presence of point defects, but still with periodic boundaries, only the dominant spatial modulation gets excited, the coupling to higher harmonics then appears lost. An even more striking effect is observed for sliders with edges: In this case, initial mode activity may instead commence at spatial modulations corresponding to the radius of the slider, the degree of which is controlled by

the edge stiffness.

Regarding applications, for which a true low-friction state with indefinite sliding is likely of most interest, the sobering news is that the system parameters must be very carefully chosen: highly harmonic interactions, small systems, defect-free. However, even if these conditions cannot be perfectly met, there is still the option to reduce friction, for example by tuning the mechanical properties of the slider edge. Interestingly, a recent publication [34] also identifies the importance of edges concerning *static* friction, so their relevance seems to extend beyond the purely *dynamic* scenarios considered here.

## ACKNOWLEDGMENTS

This work was funded by the Deutsche Forschungsgemeinschaft (DFG, German Research Foundation) – 217133147/SFB 1073, project A01.

- 
- [1] Kenneth Holmberg and Ali Erdemir, “Influence of tribology on global energy consumption, costs and emissions,” *Friction* **5**, 263–284 (2017).
  - [2] Bo N. J. Persson, *Sliding Friction* (Springer Berlin Heidelberg, 2000).
  - [3] B. N. J. Persson, E. Tosatti, D. Fuhrmann, G. Witte, and Ch. Wöll, “Low-frequency adsorbate vibrational relaxation and sliding friction,” *Physical Review B* **59**, 11777–11791 (1999).
  - [4] Yabing Qi, J. Y. Park, B. L. M. Hendriksen, D. F. Ogletree, and M. Salmeron, “Electronic contribution to friction on GaAs: An atomic force microscope study,” *Physical Review B* **77**, 184105 (2008).
  - [5] Dirk Kadau, Alfred Hucht, and Dietrich E. Wolf, “Magnetic friction in ising spin systems,” *Physical Review Letters* **101**, 137205 (2008).
  - [6] A. S. de Wijn, A. Fasolino, A. E. Filippov, and M. Urbakh, “Nanosopic friction under electrochemical control,” *Physical Review Letters* **112**, 055502 (2014).
  - [7] M. Cieplak, E. D. Smith, and M. O. Robbins, “Molecular origins of friction: The force on adsorbed layers,” *Science* **265**, 1209–1212 (1994).
  - [8] Renfeng Hu, Sergey Yu. Krylov, and Joost W. M. Frenken, “On the origin of frictional energy dissipation,” *Tribology Letters* **68** (2019), 10.1007/s11249-019-1247-7.
  - [9] Elizabeth D. Smith, Mark O. Robbins, and Marek Cieplak, “Friction on adsorbed monolayers,” *Physical Review B* **54**, 8252–8260 (1996).
  - [10] B. N. J. Persson, “Comment on “on the origin of frictional energy dissipation”,” *Tribology Letters* **68** (2020), 10.1007/s11249-020-1268-2.
  - [11] Renfeng Hu, Sergey Yu. Krylov, and Joost W. M. Frenken, “Response to comment on “on the origin of frictional energy dissipation”, by b.n.j. persson,” *Tribology Letters* **68** (2020), 10.1007/s11249-020-1280-6.
  - [12] Zhiyong Wei, Zaoqi Duan, Yajing Kan, Yan Zhang, and Yunfei Chen, “Phonon energy dissipation in friction between graphene/graphene interface,” *Journal of Applied Physics* **127**, 015105 (2020).
  - [13] Oleg M. Braun and Yuri S. Kivshar, *The Frenkel-Kontorova Model* (Springer Berlin Heidelberg, 2004).
  - [14] Jesper Norell, Annalisa Fasolino, and Astrid S. de Wijn, “Emergent friction in two-dimensional frenkel-kontorova models,” *Physical Review E* **94**, 023001 (2016).
  - [15] See Fig. 8 of Ref. [14]. The “vector” model variant, in which all higher-order terms in the particle interactions are retained, thus making it anharmonic, displays significantly higher friction.
  - [16] Richard L. C. Vink, “Connection between sliding friction and phonon lifetimes: Thermostat-induced thermolubricity effects in molecular dynamics simulations,” *Physical Review B* **100**, 094305 (2019).
  - [17] H. Schmidt, J. O. Krispeneit, N. Weber, K. Samwer, and C. A. Volkert, “Switching friction at a manganite surface using electric fields,” (2020), [arXiv:2005.08949](https://arxiv.org/abs/2005.08949) [cond-mat.mtrl-sci].
  - [18] Niklas A. Weber, Dr. Hendrik Schmidt, Tim Sievert, Prof. Christian Jooss, Dr. Friedrich Güthoff, Prof. Vasily Moshneaga, Prof. Konrad Samwer, Prof. Matthias Krüger, and Prof. Cynthia A. Volkert, “Polaronic contributions to friction in a manganite thin film,” (2020), [arXiv:2009.12137](https://arxiv.org/abs/2009.12137) [cond-mat.mtrl-sci].
  - [19] L. Consoli, H. J. F. Knops, and A. Fasolino, “Onset of sliding friction in incommensurate systems,” *Physical Review Letters* **85**, 302–305 (2000).
  - [20] L. Consoli, H. J. F. Knops, and A. Fasolino, “Breakdown of a conservation law in incommensurate systems,” *Physical Review E* **64**, 016601 (2001).
  - [21] M Peyrard and S Aubry, “Critical behaviour at the transition by breaking of analyticity in the discrete frenkel-kontorova model,” *Journal of Physics C: Solid State Physics* **16**, 1593–1608 (1983).
  - [22] Kazumasa Shinjo and Motohisa Hirano, “Dynamics of friction: superlubric state,” *Surface Science* **283**, 473–478 (1993).

- [23] Alexei Bylinskii, Dorian Gangloff, Ian Counts, and Vladan Vuletić, “Observation of aubry-type transition in finite atom chains via friction,” *Nature Materials* **15**, 717–721 (2016).
- [24] Joost A van den Ende, Astrid S de Wijn, and Annalisa Fasolino, “The effect of temperature and velocity on superlubricity,” *Journal of Physics: Condensed Matter* **24**, 445009 (2012).
- [25] Martin Dienwiebel, Gertjan S. Verhoeven, Namboodiri Pradeep, Joost W. M. Frenken, Jennifer A. Heimberg, and Henny W. Zandbergen, “Superlubricity of graphite,” *Physical Review Letters* **92**, 126101 (2004).
- [26] Astrid S. de Wijn, Annalisa Fasolino, A. E. Filippov, and M. Urbakh, “Low friction and rotational dynamics of crystalline flakes in solid lubrication,” *EPL (Europhysics Letters)* **95**, 66002 (2011).
- [27] M. S. Tomassone, J. B. Sokoloff, A. Widom, and J. Krim, “Dominance of phonon friction for a xenon film on a silver (111) surface,” *Physical Review Letters* **79**, 4798–4801 (1997).
- [28] A. Benassi, A. Vanossi, G. E. Santoro, and E. Tosatti, “Parameter-free dissipation in simulated sliding friction,” *Physical Review B* **82**, 081401 (2010).
- [29] A. Benassi, A. Vanossi, G. E. Santoro, and E. Tosatti, “Optimal energy dissipation in sliding friction simulations,” *Tribology Letters* **48**, 41–49 (2012).
- [30] Irina V. Lebedeva, Andrey A. Knizhnik, Andrey M. Popov, Yurii E. Lozovik, and Boris V. Potapkin, “Interlayer interaction and relative vibrations of bilayer graphene,” *Physical Chemistry Chemical Physics* **13**, 5687 (2011).
- [31] Christian Apostoli, Giovanni Giusti, Jacopo Ciccianni, Gabriele Riva, Rosario Capozza, Rosalie Laure Woulaché, Andrea Vanossi, Emanuele Panizon, and Nicola Manini, “Velocity dependence of sliding friction on a crystalline surface,” *Beilstein Journal of Nanotechnology* **8**, 2186–2199 (2017).
- [32] Steve Plimpton, “Fast parallel algorithms for short-range molecular dynamics,” *Journal of Computational Physics* **117**, 1–19 (1995).
- [33] T. S. van Erp, A. Fasolino, O. Radulescu, and T. Janssen, “Pinning and phonon localization in frenkel-kontorova models on quasiperiodic substrates,” *Physical Review B* **60**, 6522–6528 (1999).
- [34] Nicola Varini, Andrea Vanossi, Roberto Guerra, Davide Mandelli, Rosario Capozza, and Erio Tosatti, “Static friction scaling of physisorbed islands: the key is in the edge,” *Nanoscale* **7**, 2093–2101 (2015).
- [35] József Cserti and Géza Tichy, “A simple model for the vibrational modes in honeycomb lattices,” *European Journal of Physics* **25**, 723–736 (2004).

### Appendix A: MD implementation details

Both the 1D and 2D model can be implemented in LAMMPS [32] using mainly standard features (the exception is the anharmonic bond potential of Eq. (1), for which we modified an existing bond style). All data were obtained in the microcanonical ensemble (`fix nve`, `timestep 0.001`). For the rigid flake, `fix rigid/nve` was used to implement the rigid edge. The essential sim-

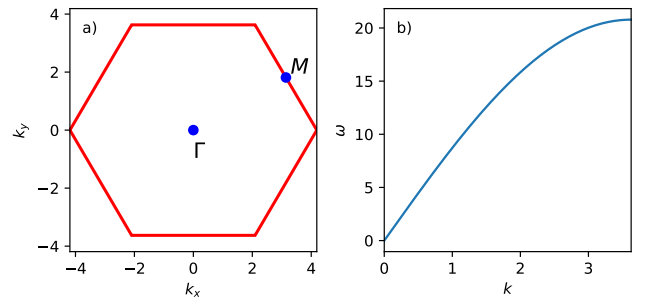


FIG. 9. a) FBZ of the hexagonal lattice. b) Longitudinal dispersion along the line  $\Gamma M$ .

ulation output is the trajectory, i.e. particle positions and velocities as a function of time, from which all quantities of interest can be computed. For the computation of the hessian and eigenmodes, a dedicated C-code was used, based on LAPACK. This code was also used to process the MD trajectory, in order to obtain the mode kinetic energy and amplitude.

### Appendix B: Coherent distribution

In the strict absence of phonon scattering, the quantity  $\vec{v}_i(t) \cdot \vec{\xi}_{k,i}$  in Eq. (3) is a periodic function at the eigenfrequency  $\omega_k$ , implying for the kinetic energy  $K_k(t) = K_{0,k} \cos^2(\omega_k t + \phi_k)$ , with amplitude  $K_{0,k}$ , and phase  $\phi_k$ . Converting the time series signal  $K_k(t)$  into a histogram, the inverse height of the bin corresponding to the energy value  $K_k$  will be given by

$$\frac{1}{H(K_k)} \propto \left| \frac{dK_k}{dt} \right| \propto \sqrt{K_k(K_{0,k} - K_k)} \approx c\sqrt{K_k}, \quad (\text{B1})$$

with  $c$  a constant, and where the approximation refers to the limit of small  $K_k$ , which Eq. (5) uses. If one does not make this approximation, then the histogram  $H(K_k)$  will actually reveal two peaks, at  $K_k = 0, K_{0,k}$ . For the 1D chain *without* the external field, which then is a true harmonic system where phonon scattering is strictly absent, this is indeed what one observes. However, in the presence of the external field (induced by the static obstacles), we never observed the second high-energy peak, since this peak is then exponentially suppressed by the Maxwell-Boltzmann factor.

### Appendix C: Dispersion relation hexagonal lattice

With the hexagonal sliding lattice oriented in the  $(xy)$ -coordinate system as shown in Fig. 1(a), the first Brillouin zone (FBZ) is a hexagon oriented as shown in Fig. 9(a), where  $\Gamma M = 2\pi/(\sqrt{3}a)$  indicates the  $+30^\circ$  propagation direction. Fig. 9(b) shows the longitudinal

dispersion along  $\Gamma M$ , with  $\omega$  expressed in the units of our model. The dispersion relation was computed numerically using equations provided in Ref. [35]. For val-

ues of  $k$  outside the interval  $\Gamma M$ , one uses the *periodic even extension* of the dispersion relation to obtain the frequency.